Supporting information

Manipulation of chemistry behaviors of species by temperature-program strategy: Efficiently confining the metal oxide nanoclusters size in hollow zeolite

Yi Zhai,[a,#] Kaiwei Wang,[a,#] Mingshuai Sun,[b*] Fumin Wang,[a*] Xubin Zhang,[a*] Guojun Lv,[c] Linfang Jiang,[a] Zhibo Xu,[a]

[a]*School of Chemical Engineering and Technology, Tianjin University, Tianjin 300350, P.R. China*

[b]*National Engineering Research Center for Carbohydrate Synthesis, Key Laboratory of Fluorine and Silicon for Energy Materials and Chemistry of Ministry of Education, College of Chemistry and Chemical Engineering, Jiangxi Normal University, Nanchang 330022 China*

[c]*School of Environmental and Chemical Engineering, Jiangsu University of Science and Technology, Zhenjiang 212003, Jiangsu, P.R. China*

*Corresponding authors: mingshuaisun@jxnu.edu.cn (Mingshuai Sun)

wangfumin@tju.edu.cn (Fumin Wang)

tjzxb@tju.edu.cn (Xubin Zhang)

# Yi Zhai and Kaiwei Wang contributed equally.

Fax: +86 22789041; Tel: +86 22789041.

Notes:

The authors declare no competing financial interest.

Computational details

DFT calculations were implemented in CASTEP package using GGA functional in the form of PBE [1-4]. Fe_2O_3 (104) and CuO (111) surface was cleaved from bulk Fe_2O_3 and CuO respectively. A 4×2×1 supercell with a vacuum slab in thickness of 15 Å was created for reaction of silanols on CuO (111) surface, and a 2×2×1 supercell with same thickness was created for the reaction on CuO (111) surface. The convergence tolerance for geometry optimization was conducted in fine quality. A custom cutoff energy of 400 eV was adopted and the SCF tolerance of 1.0×10^{-6} eV/atom were applied in the computations. The k-point mesh of Brillouin zone was set to be Gamma for geometry optimization and transition state search. The reactions between silanols with different numbers of silicon atoms are calculated in a supercell of similar size (14.8 Å×10.0 Å×20.0 Å) and using the same calculation parameters. All transition states were located by performing complete LST/QST calculations [5, 6].

[1] S.J. Clark, M.D. Segall, C.J. Pickard, P.J. Hasnip, M. Probert, K. Refson, M.C. Payne, First principles methods using CASTEP, Z. Kristallogr., (2005) 567-570.
[2] W. Kohn, L.J. Sham, Self-consistent equations including exchange and correlation effects, Phys. Rev., 140 (1965) A1133.
[3] J.P. Perdew, K. Burke, M. Ernzerhof, Generalized gradient approximation made simple, Phys. Rev. Lett., 77 (1996) 3865.
[4] G. Kresse, D. Joubert, From ultrasoft pseudopotentials to the projector augmented-wave method, Physical review b, 59 (1999) 1758.
[5] T.A. Halgren, W.N. Lipscomb, The synchronous-transit method for determining reaction pathways and locating molecular transition states, Chem. Phys. Lett., 49 (1977) 225-232.
[6] N. Govind, M. Petersen, G. Fitzgerald, D. King-Smith, J. Andzelm, A generalized synchronous transit method for transition state location, Computational materials science, 28 (2003) 250-258.

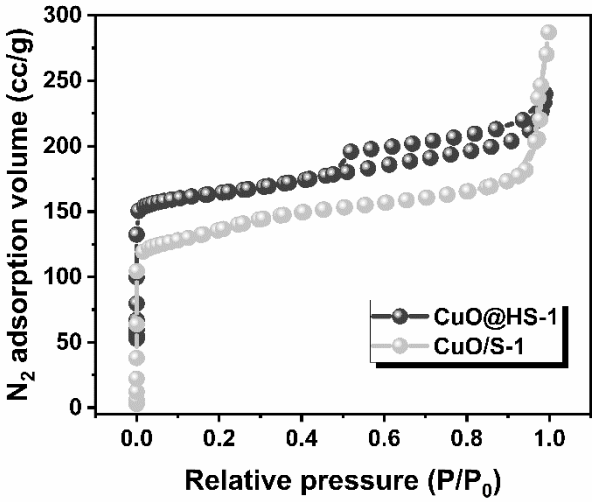

Figure S1. (d) N_2 adsorption-desorption isotherms of CuO@HS-1 and CuO/S-1.

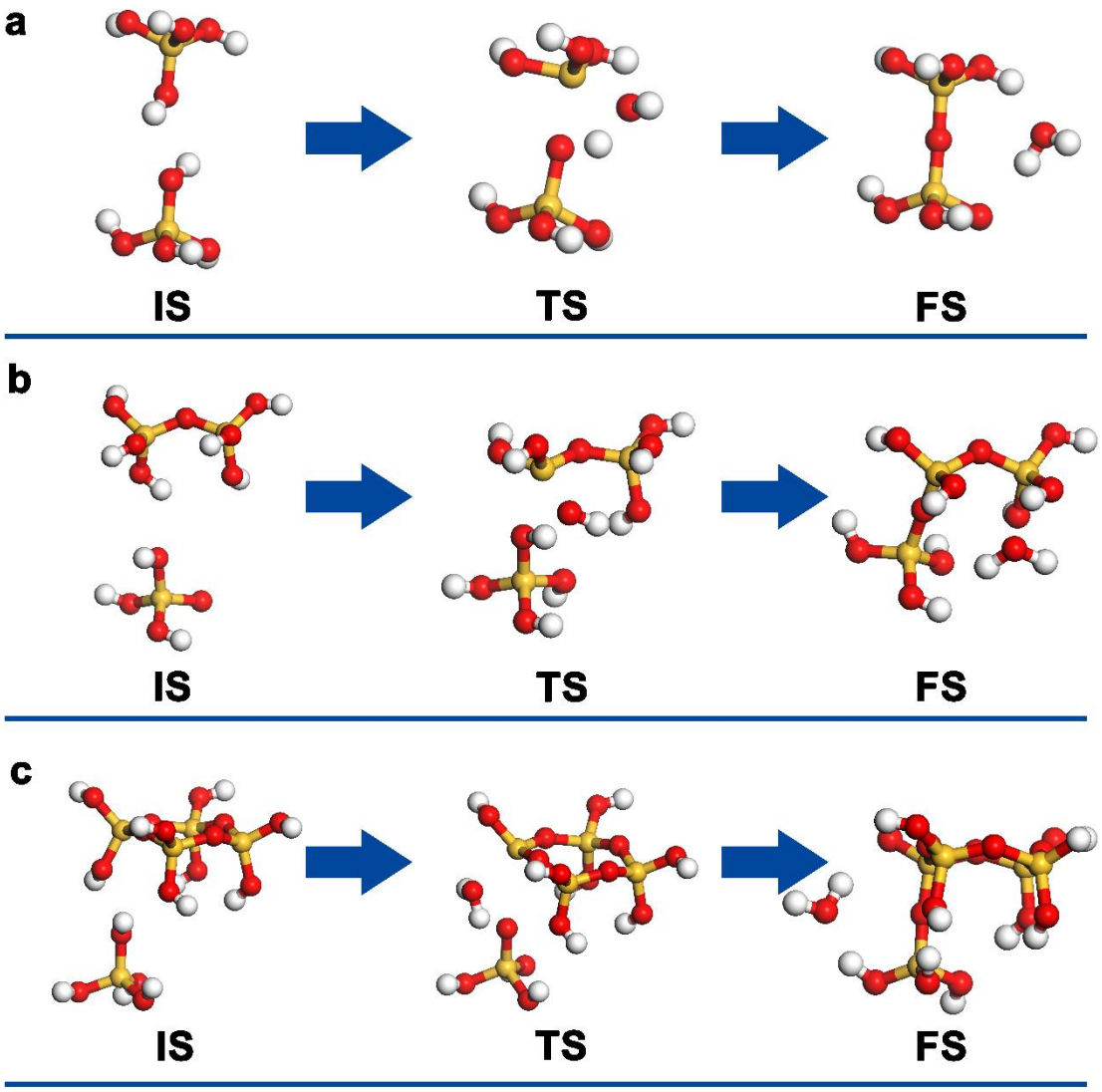

Figure S2. The condensation reactions route between unsaturated silicon species (Q^0, Q^1, Q^2) with $Si(OH)_4$ species: (a) Q^0, (b) Q^1 and (c) Q^2. Oxygen atom (red), Silica atom (yellow) and Hydrogen atom (white)

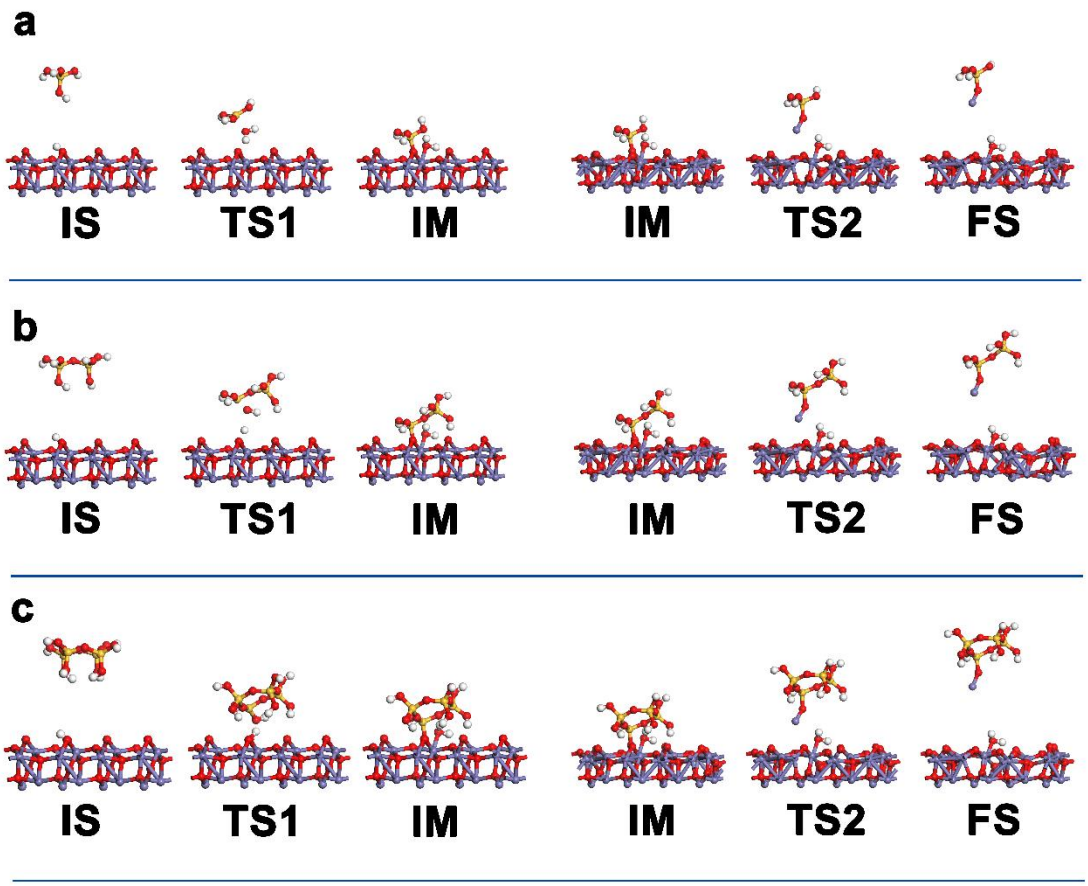

Figure S3. The condensation reactions route between unsaturated silicon species (Q^0, Q^1, Q^2) with Fe-OH species in Fe_2O_3 phase: (a) Q^0, (b) Q^1 and (c) Q^2. Oxygen atom (red), Silica atom (yellow), Hydrogen atom (white) and iron atom (purple).

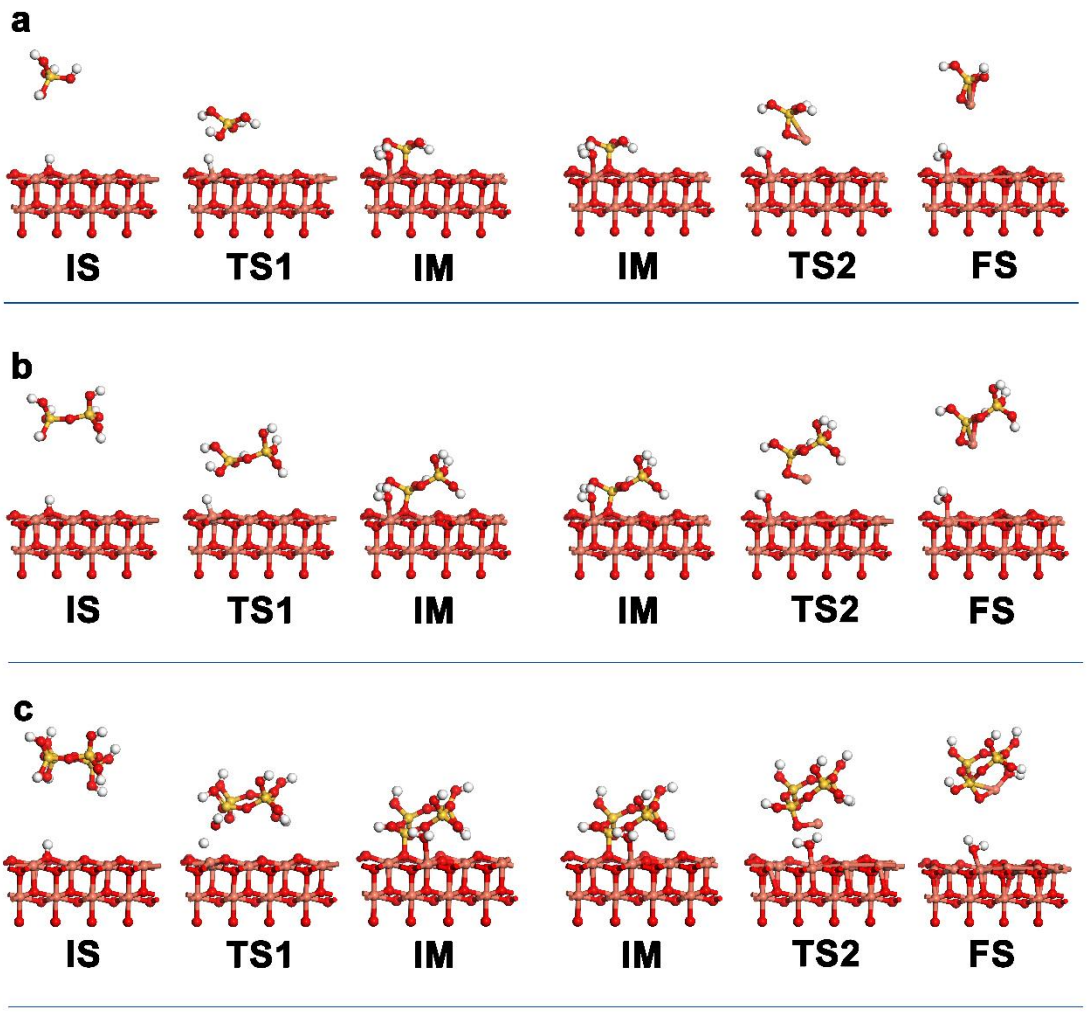

Figure S4. The condensation reactions route between unsaturated silicon species (Q^0, Q^1, Q^2) with Cu-OH species in CuO phase: (a) Q^0, (b) Q^1 and (c) Q^2. Oxygen atom (red), Silica atom (yellow), Hydrogen atom (white) and copper atom (orange).

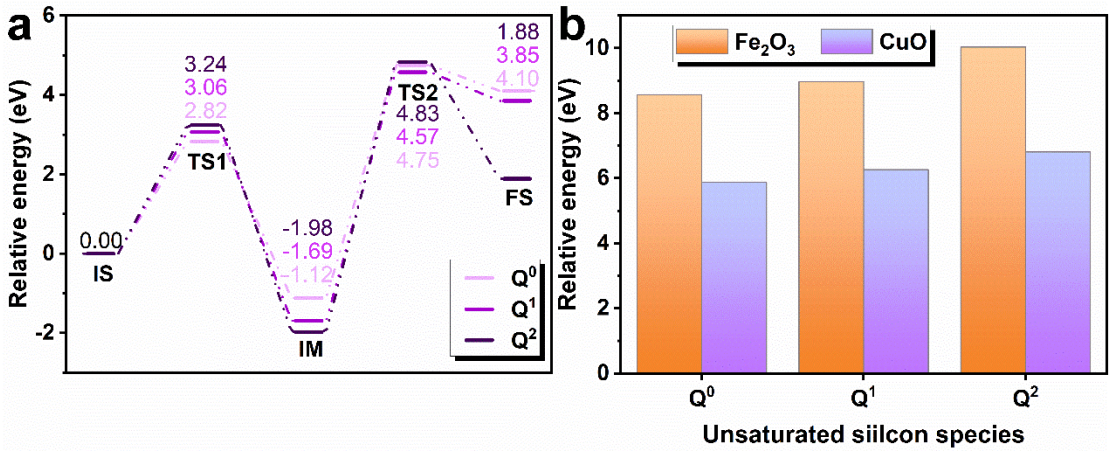

Figure S5. (a) Energy profile of the unsaturated silicon species (Q^0, Q^1, Q^2) reaction with CuO phase. (b) Corresponding energies of the formation of Si-O-Fe and Si-O-Cu bonds by the condensations of unsaturated silicon species (Q^0, Q^1, Q^2) with and Fe_2O_3 phase and CuO phase.

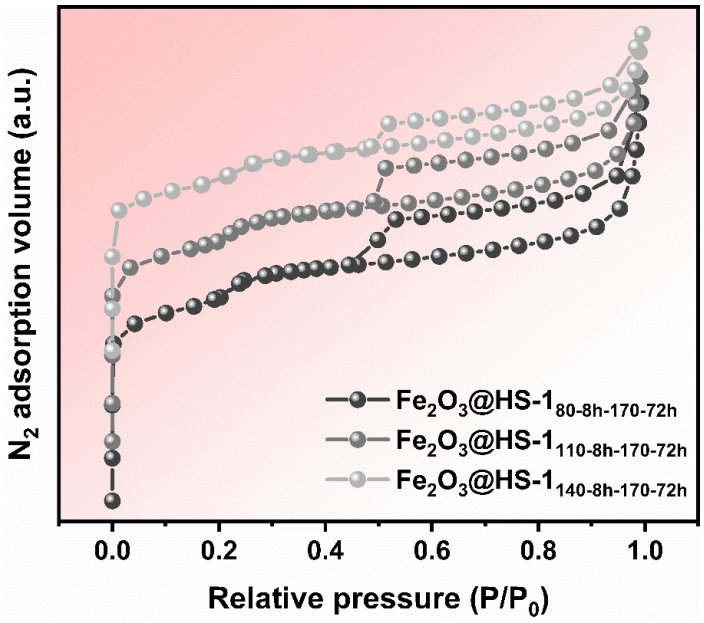

Figure S6. N_2 adsorption-desorption isotherms of samples synthesized at different temperature program.

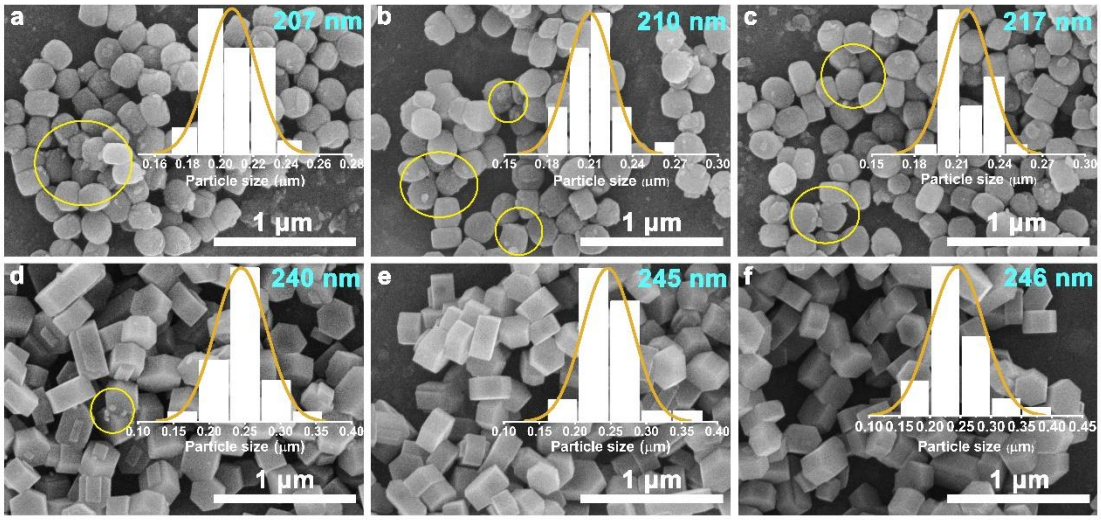

Figure S7. SEM images of at Fe_2O_3@HS-1 synthesized at different times and corresponding particle size distributions: (a) 0 h; (b) 2 h; (c) 8 h; (d) 32 h; (e) 56h and (f) 80 h

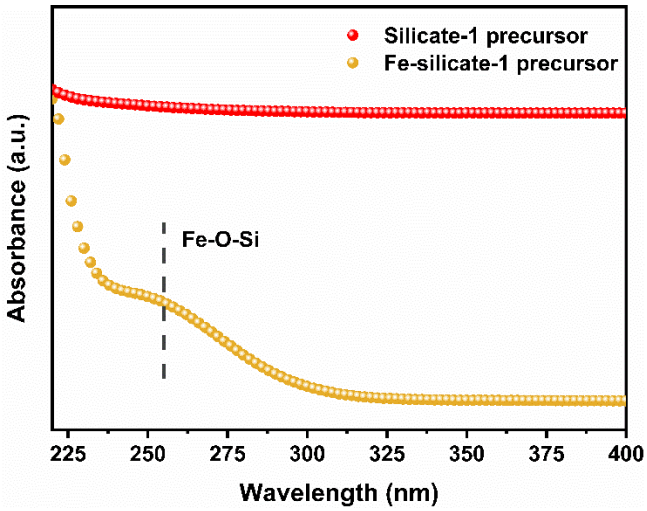

Figure S8. UV-vis spectra of at zeolite precursors.

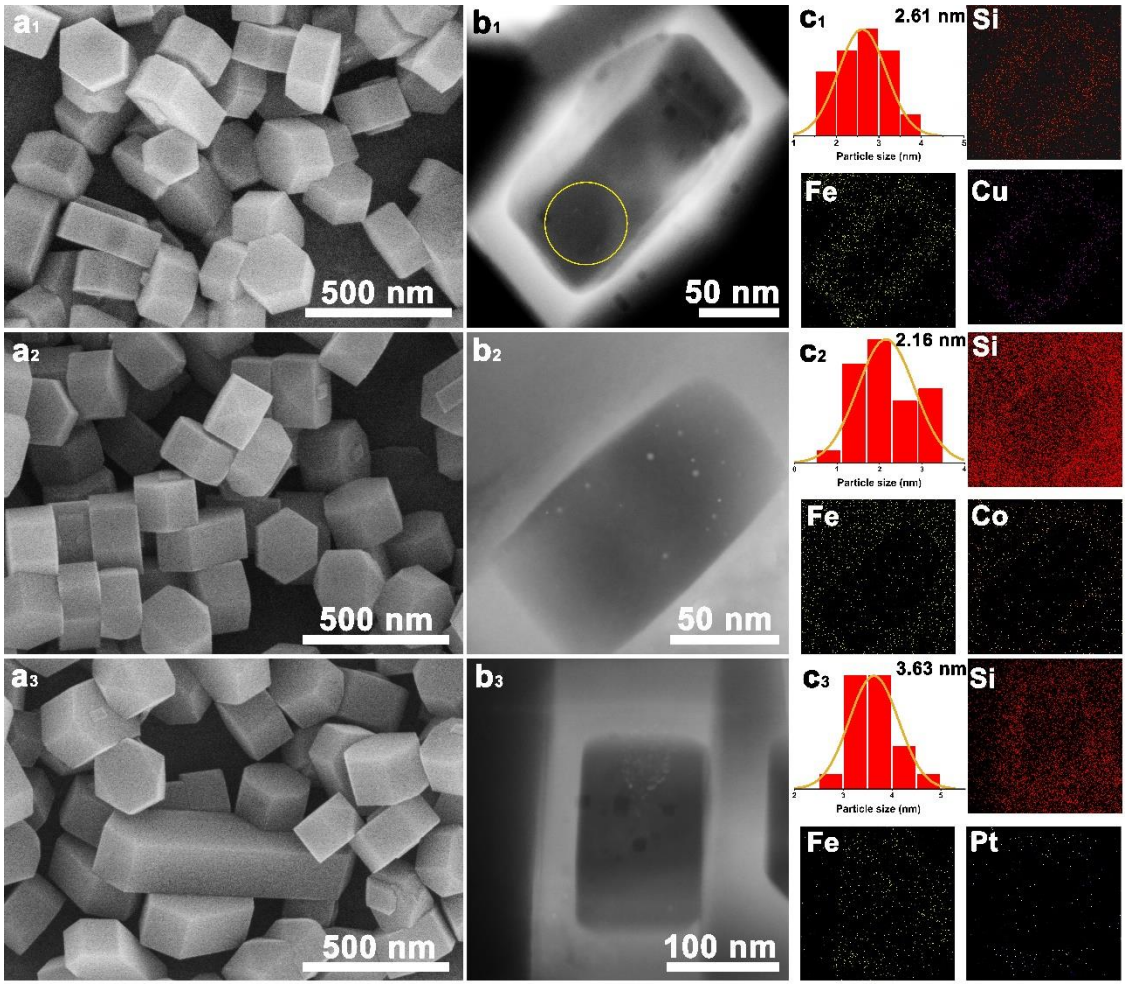

Figure S9. (a) SEM images, (b) TEM images with corresponding elements-mapping and (c) metal oxides clusters size distributions: 1, $1Fe_2O_3$-1CuO@HS-1; 2, Fe_2O_3-$1CoO_x$@HS-1 and 3, $1Fe_2O_3$-$1PtO_x$@HS-1.

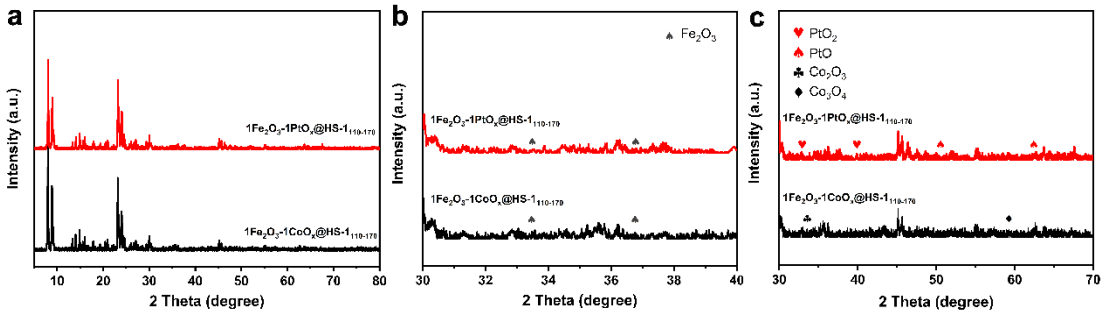

Figure S10. XRD patterns of $1Fe_2O_3$-$1CoO_x$@HS-1 and $1Fe_2O_3$-$1PtO_x$@HS-1.

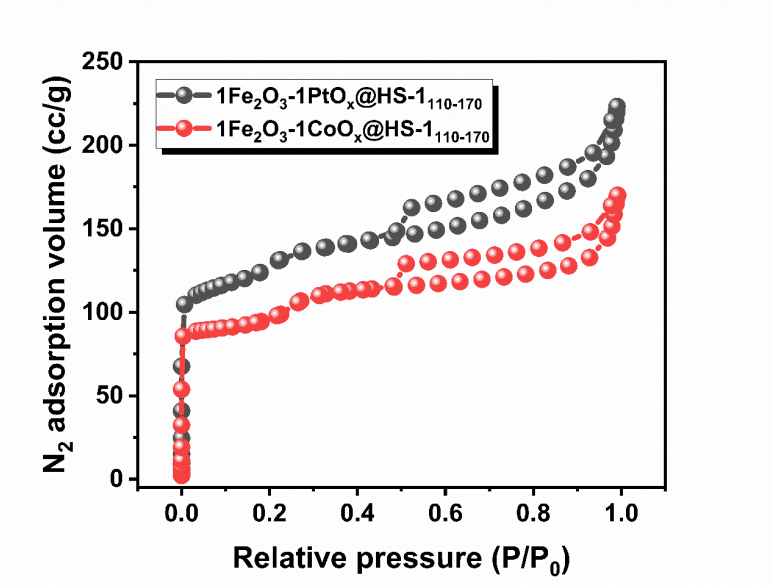

Figure S11. N_2 adsorption-desorption isotherms of $1Fe_2O_3$-$1CoO_x$@HS-1 and $1Fe_2O_3$-$1PtO_x$@HS-1.

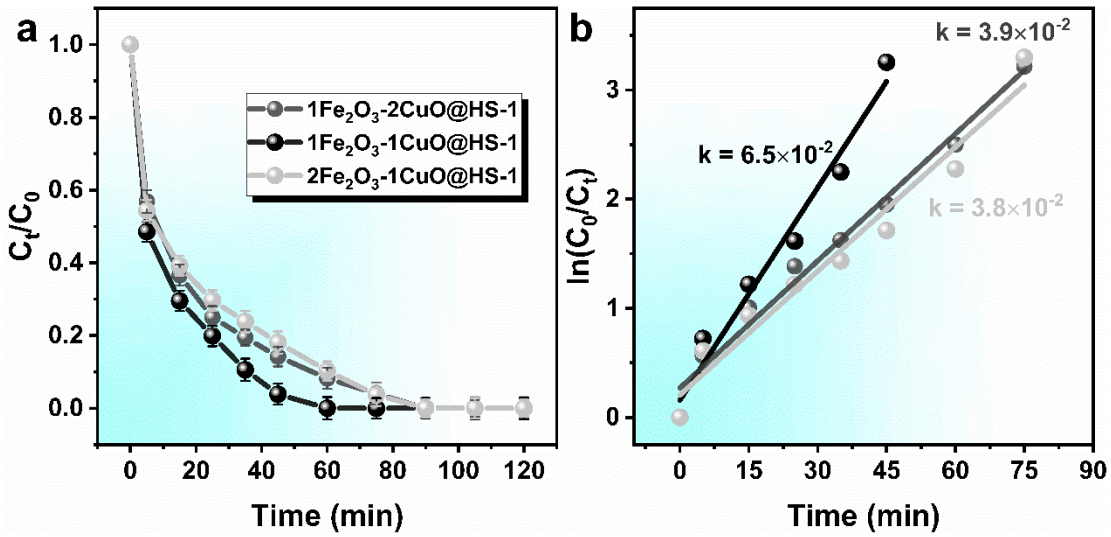

Figure S12. (a) The phenol degradation and (b) Kinetic constants catalyzed by samples with different Fe/Cu molar ratios.

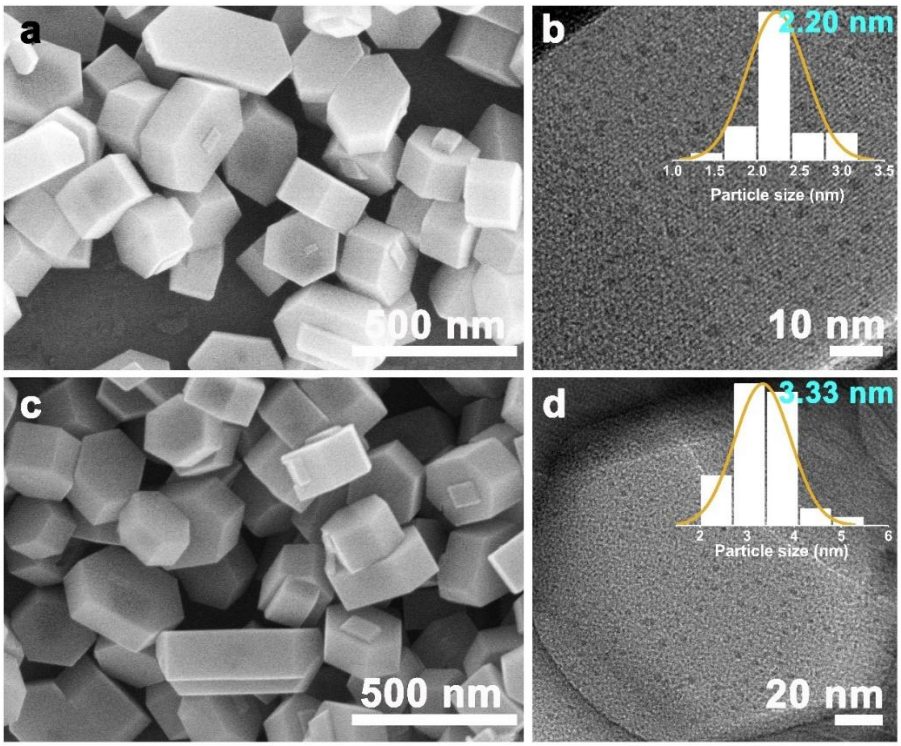

Figure S13. (a) SEM images and (b) TEM images with corresponding metal oxide clusters size of recycled Fe_2O_3@HS-1 after 5 cycle experiments. (c) SEM images and (d) TEM images with corresponding metal oxide clusters size of recycled 1Fe_2O_3-1CuO@HS-1 after 5 cycle experiments.

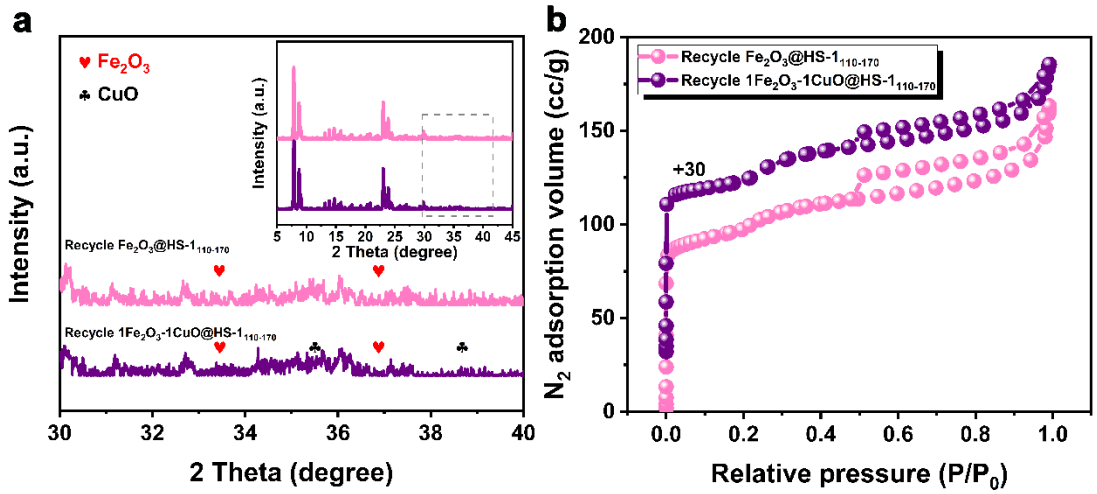

Figure S14. (a) XRD patterns and (b) N_2 adsorption-desorption isotherms of recycled Fe_2O_3@HS-1 after 5 cycle experiments.

Table S1. Textual parameters of synthesized zeolites at various synthetic conditions

sample	S_{BET}[a] (m^2/g)	S_{ext}[b] (m^2/g)	V_{micro}[b] (cm^3/g)	V_{meso}[c] (cm^3/g)	V_{total}[d] (cm^3/g)
Fe_2O_3/S-1	418.06	23.48	0.203	0.104	0.257
Fe_2O_3@HS-1$_{80\text{-}8h\text{-}170\text{-}72h}$	390.45	33.45	0.182	0.195	0.318
Fe_2O_3@HS-1$_{140\text{-}8h\text{-}170\text{-}72h}$	337.11	33.09	0.157	0.151	0.259
Fe_2O_3@HS-1$_{110\text{-}2h\text{-}170\text{-}0h}$	382.35	48.05	0.181	0.275	0.412
Fe_2O_3@HS-1$_{110\text{-}8h\text{-}170\text{-}0h}$	374.59	48.29	0.174	0.335	0.462
Fe_2O_3@HS-1$_{110\text{-}8h\text{-}170\text{-}24h}$	364.63	31.62	0.169	0.216	0.329
Fe_2O_3@HS-1$_{110\text{-}8h\text{-}170\text{-}48h}$	361.74	33.01	0.170	0.177	0.290
Fe_2O_3@HS-1$_{110\text{-}8h\text{-}170\text{-}72h}$	363.50	35.49	0.174	0.171	0.290
CuO/S-1	438.74	22.07	0.212	0.140	0.382
CuO@HS-1$_{110\text{-}8h\text{-}170\text{-}72h}$	370.64	38.60	0.166	0.158	0.294
1Fe_2O_3-1CuO/S-1	371.94	30.83	0.177	0.114	0.262
1Fe_2O_3-1CuO@HS-1$_{110\text{-}8h\text{-}170\text{-}72h}$	336.67	33.18	0.157	0.148	0.250
1Fe_2O_3-1PtO_x@HS-1$_{110\text{-}8h\text{-}170\text{-}72h}$	345.75	32.46	0.160	0.159	0.251
1Fe_2O_3-1CoO_x@HS-1$_{110\text{-}8h\text{-}170\text{-}72h}$	355.60	35.96	0.163	0.165	0.244

[a]Measured from multipoint BET method; [b]Measured from t-plot method; [c]V_{meso} calculated by using BJH method, [d]Determined from adsorbed volume at P/P_0=0.99.

Table S2. The content of various iron species for different samples

sample	Total[a] (wt%)	245 nm[b] (wt%)	250-300 nm[b] (wt%)	300-400 nm[b] (wt%)	Above 400 nm[b] (wt%)
Fe_2O_3/S-1	2.670	0.288	0.185	1.406	0.791
Fe_2O_3@HS-1$_{80\text{-}8h\text{-}170\text{-}72h}$	2.079	0.432	0.096	1.370	0.181
Fe_2O_3@HS-1$_{140\text{-}8h\text{-}170\text{-}72h}$	2.191	0.438	0.174	1.308	0.271
Fe_2O_3@HS-1$_{110\text{-}2h}$	2.341	0.219	0.118	1.353	0.651
Fe_2O_3@HS-1$_{110\text{-}8h}$	2.140	0.208	0.138	1.181	0.613
Fe_2O_3@HS-1$_{110\text{-}8h\text{-}170\text{-}24h}$	2.125	0.387	0.123	1.396	0.219
Fe_2O_3@HS-1$_{110\text{-}8h\text{-}170\text{-}48h}$	2.196	0.411	0.119	1.521	0.145
Fe_2O_3@HS-1$_{110\text{-}8h\text{-}170\text{-}72h}$	2.180	0.458	0.129	1.464	0.129

[a]Measured by ICP-OES; [b]Calculated by combining with UV-vis spectra and ICP-OES